





Cite this: DOI: 10.1039/d5im00014a

Synthesis and properties of symmetric glycerol-derived (*E/Z*)-1,3-diether-2-alkenes†

Jun Wang, Shuai Qian, Gbolagade Olajide, Sourav Chatterjee,
Tibor Szilvási  and Jason E. Bara *

The synthesis of new and potentially “green” solvents and other small molecules/intermediates from glycerol and associated derivatives is promising for expanding glycerol valorization. Previously, we showed that eliminating H-bonding reduces solvent–solvent interactions and increases CO₂ solubility in 1,3-diether-2-ketones compared to 1,3-diether-2-alcohols based on glycerol skeletons. Further exploration of glycerol-derived 1,3-diether-2-propanol compounds into corresponding 1,3-diether-2-alkenes can yield valuable insights into structure–property relationships as well as new chemical intermediates. In the current work five symmetric glycerol-derived (*E/Z*)-1,3-diether-2-alkenes were synthesized: 1,3-dimethoxyprop-1-ene ([M, A, M]), 1,3-diethoxyprop-1-ene ([E, A, E]), 2,5,9,12-tetraoxatridec-6-ene ([ME, A, ME]), 1,3-bis(2,2,2-trifluoromethoxy)prop-1-ene ([F, A, F]), and prop-1-ene-1,3-diylbis(oxy)bis(methylene)dibenzene ([Bn, A, Bn]), using a three-step strategy starting from epichlorohydrin. All compounds were purified using thorough distillation and drying methods. The *E*:*Z* ratio in all products was close to 1:1. Thermophysical properties of the synthesized (*E/Z*)-1,3-diether-2-alkenes (e.g., density, refractive index, viscosity) were measured over the range of *T* = 293.15–333.15 or 343.15 K. CO₂ absorption capacities (Henry’s constants) of [F, A, F] were measured at *T* = 303.15, 318.15, 333.15, and 348.15 K and pressures in the range of *P* = 2–10 atm. Density, viscosity, vapor pressure, enthalpy of vaporization, and dipole moment were also calculated for each compound. Additionally, it was demonstrated that the C=C bond remains accessible for further reactions and can undergo bromination and thus may also have applications as intermediates for more complex molecules that are based on glycerol skeletons.

Received 23rd January 2025,
Accepted 6th May 2025

DOI: 10.1039/d5im00014a

rsc.li/icm

Keywords: Glycerol; Green solvents; CO₂ absorption; Symmetric alkenes; Platform molecules.

1 Introduction

Glycerol constitutes ~10% by mass of the reaction products obtained from the transesterification of animal fats and vegetable oils in biodiesel production, and is a versatile polyol widely used in various industries,^{1–3} including food, pharmaceuticals, personal care, and cosmetics.^{4,5} The rapid expansion of the biodiesel sector has led to a surplus of glycerol,⁶ requiring innovative valorization strategies. Crude glycerol generally requires upgrading (e.g., distillation), and the supply far exceeds the demand for high-purity glycerol. Broader uses for glycerol as a solvent are hindered by its high viscosity and water uptake. Converting glycerol to epichlorohydrin (ECH), glycidol, or glycidyl ethers transforms it into “activated forms”,^{7,8} which can expedite access to novel “green” solvents,⁹ chemical building blocks, monomers, and

polymers. “Green chemistry” is increasingly recognized as an essential component of sustainable chemical design and synthesis, with solvents playing a critical role in ensuring environmental compatibility.^{10,11} Many organic solvents are derived from petroleum, which poses significant risks to both human health and the environment. The synthesis of valuable glycerol-derived solvents from “activated forms” of molecules could create new applications that utilize surplus glycerol, while also providing safer, biodegradable alternatives to conventional organic solvents.

Oxygenated compounds are essential for advancing fuel additives,¹² where glycerol ether derivatives are advantageous as they contribute to the recycling of the abundant glycerol stocks.¹³ Beyond their application as fuel additives, small-molecule glycerol ether derivatives are promising candidates for next-generation CO₂ capture solvents.¹⁴ These compounds exhibit low viscosity, sustainable sources, and dense ether functional groups, providing exceptional CO₂ affinity relative to many other “physical” organic solvents.

Utilizing ECH or glycidyl ethers as starting materials for “green solvents” with glycerol skeletons presents the

Dept. of Chemical & Biological Engineering, The University of Alabama,
Tuscaloosa, AL, 35487-0203, USA. E-mail: jbara@eng.ua.edu

† Electronic supplementary information (ESI) available. See DOI: <https://doi.org/10.1039/d5im00014a>



opportunity to selectively synthesize various small molecules with tailored properties, some of which may be suitable for CO₂ absorption processes.^{15–19} Previous studies have explored the synthesis of glycerol ethers in the forms of 1,3-diether-2-alcohols,^{20,21} 1,3-diether-2-ketones,^{22,23} and 1,2,3-triethers,^{23,24} indicating that etherified glycerol derivatives possess diverse and tunable properties. We also showed that the secondary (2°) alcohol present in 1,3-diether-2-alcohols could be efficiently converted to the corresponding –Cl or –Br (*i.e.*, halide) or mesylate (–OMs) forms, thereby potentially activating the central C atom in glycerol.²⁵ This led us to consider whether instead of using these compounds as electrophiles (as in the synthesis of imidazolium ionic liquids (ILs)), we could utilize this functionalization strategy to form alkenes *via* elimination reactions.

Bio-olefins present a promising opportunity in the market, largely attributable to their renewable sources and the environmental benefits they offer in comparison to traditionally produced olefins.²⁶ They are essential raw materials in manufacturing plastics, detergents, adhesives, rubber, and food packaging.²⁷ However, research in the area of glycerol-derived alkenes has not yet been fully investigated. To address this gap, we investigated glycerol-derived 1,3-diether-2-alkenes for their potential applications.

In these studies, five symmetric (*E/Z*)-1,3-diether-2-alkenes were synthesized through a three-step reaction starting from ECH, where the *E:Z* product ratio was close to 1:1 (Table 1). Huang *et al.*²⁸ synthesized *Z*-[M, A, M] (44% yield) for the first time and employed them in an inverse-electron-demand Diels–Alder reaction for racemic and achiral total synthesis. Hall *et al.*²⁹ used 1,1,3-trialkoxypropanes for thermal fission to synthesize α,β -

unsaturated aldehydes, and yielding *E*-[E, A, E] at 50%. Gould synthesized 1,3-dibutoxyprop-1-ene from the *p*-toluenesulfonate (*i.e.* tosylate, –OTs) of 1,4-dibutoxy-2-propanol and reported an *E:Z* ratio of 1:4.³⁰ Gould showed that the alkene could be reacted with *t*-butyl lithium (forming a vinyl anion) and then alkylated at the vinyl position with iodomethane. In addition to this reaction, these alkenes can serve as intermediates for bromination and oxidation,³¹ and thus can provide unique intermediates for synthesizing molecules using glycerol-derived C atoms.

We aim to investigate how adding alkyl groups alters the properties from [M, A, M] to [E, A, E]. Similar R groups were selected for [ME, A, ME] and [F, A, F] based on our previous study,^{20,22,23} which showed that additional ether groups and F atoms improve the solvent's CO₂ absorption capacity. The benzyl (aromatic ring) R group was chosen because it acts as a weak electron-donating group (EDG) and is being investigated by our group for the first time. Table 1 details the compounds developed in this work. Density and viscosity were measured as a function of temperature, followed by refractive index (RI) measurements at *T* = 293.15 K and 298.15 K. Furthermore, as both ether³² and fluorinated³³ groups have demonstrated superior qualities for CO₂ absorption, the relationship between CO₂ solubility and temperature (*T* = 303.15, 318.15, 333.15, and 348.15 K) and pressure (*P* = 2–10 atm) for [F, A, F] was evaluated. This study reports the thermophysical and thermodynamic properties of (*E/Z*)-1,3-diether-2-alkenes for the first time. Computational studies were also conducted to compare experimental density and viscosity results, along with predictions of dipole moments, enthalpies of vaporization, and vapor pressures.

Table 1 Names, formulas, structures, acronyms, ratios, and CAS registry numbers of symmetric compounds studied in this work

IUPAC name	Formula	Structure (<i>E/Z</i>)	Ratio	Acronym/CAS #
(<i>E/Z</i>)-1,3-Dimethoxyprop-1-ene	C ₅ H ₁₀ O ₂		47 : 53	[M, A, M] (<i>E</i>) 80355-36-8
(<i>E/Z</i>)-1,3-Diethoxyprop-1-ene	C ₇ H ₁₄ O ₂		49 : 51	[E, A, E] (<i>E</i>) 97729-23-2
(<i>E/Z</i>)-2,5,9,12-Tetraoxatridec-6-ene	C ₉ H ₁₈ O ₄		40 : 60	[ME, A, ME] N/A
(<i>E/Z</i>)-1,3-Bis(2,2,2-trifluoroethoxy)prop-1-ene	C ₇ H ₈ F ₆ O ₂		46 : 54	[F, A, F] N/A
(<i>E/Z</i>)-((Prop-1-ene-1,3-diylbis(oxy))bis(methylene))dibenzene	C ₁₇ H ₁₈ O ₂		45 : 55	[Bn, A, Bn] N/A



2 Results and discussion

2.1 Efficiency of the synthesis method

This study focused on the synthesis of five symmetric (*E/Z*)-1,3-diether-2-alkenes ($[R_1, A, R_1]$) using a three-step strategy at the molar scale, as illustrated in Scheme 1. The synthesis process begins with forming the symmetric glycerol 1,3-diether ($[R_1, O, R_1]$) from ECH and an excess of the corresponding primary (1°) alcohol, using methods similar to those in our previous work.^{17,34} The -OH group of the central glycerol C atom is then functionalized with methanesulfonyl chloride (MsCl) to form $[R_1, Ms, R_1]$. In the final step, the -OMs group serves as an effective leaving group, facilitating the elimination reaction to form the C=C double bond. The symmetric $[R_1, Ms, R_1]$ structure and mechanism of a β -H elimination, results in an *E:Z* ratio of approximately 1:1 for all compounds. (Table 1). It is also worth mentioning that an elimination reaction was attempted with $[2F, Ms, 2F]$ (as synthesized from the reaction between hexafluoroisopropanol (HFIP) and ECH), but did not yield $[2F, A, 2F]$. The $[2F, Ms, 2F]$ on both sides contain two strong electron-withdrawing groups (EWGs) that caused the 1,4-elimination reaction, and only by-products were obtained from these types of intermediates. The five symmetric (*E/Z*)-1,3-diether-2-alkenes obtained were hydrophobic which benefits the post-reaction process by improving product purity and yield. The isolated yields of the overall three-step reactions for $[M, A, M]$, $[E, A, E]$, $[ME, A, ME]$, $[F, A, F]$, and $[Bn, A, Bn]$ were 30.3%, 35.9%, 56.8%, 53.8%, and 61.7%, respectively. It is essential to limit the exposure to vacuum during the purification of $[M, A, M]$ and $[E, A, E]$ due to their volatility.

2.2 Solvent densities

The densities of the five symmetric (*E/Z*)-1,3-diether-2-alkenes and $[F, Br_2, F]$ were measured and calculated, with results presented in Table 2 and plotted in Fig. 1. The linear regression equations for each compound (constants in Table 3) yielded $R^2 = 1.000$, with a maximum deviation of <0.01%. This precision allows density predictions at temperatures beyond the experimental data, which is crucial for calculating the CO₂ absorption capacities in organic liquids.³⁵ An attempt was made to compare the density and viscosity of these alkenes with the corresponding

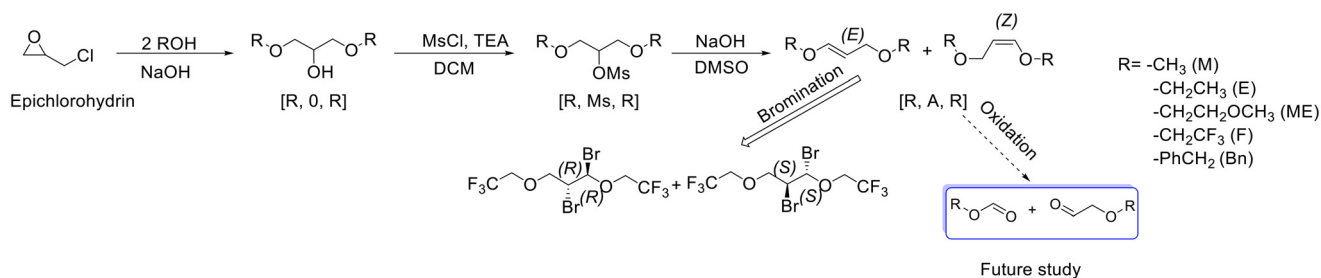
aliphatic ethers. However, while the syntheses of 1,3-dimethoxypropane, 1,3-diethoxypropane, and 1,1-[1,3-propanediylbis(oxyethylene)]bis[benzene] exist in the literature, no density or viscosity data exist.

As expected, density decreases with increasing temperature due to volume expansion from increased molecular motion. To augment the experimentally measured thermophysical properties of the studied liquid products and gain deeper insight beyond the measured values, we employed the COSMOtherm software package (BIOVIA COSMOtherm, released 2020).^{36,37} This software has proven to be an effective and practical tool for predicting the physical properties of similar liquids, ensuring the reliability and accuracy of our comparative analysis.^{23–25} COSMOtherm calculations for the *E* (ρ_c) and *Z* (ρ_d) structures over the range of $T = 293.15$ – 343.15 K, shown in Table 2, exhibited the same trend and closely matched measured values, with a maximum absolute percentage error of -7.2%. These calculated densities closely align with the experimental data for all studied compounds at all selected temperatures, with the absolute error ranging from 0.01% for *Z*- $[M, A, M]$ at 343.15 K to 7.64% for *S*- $[F, Br_2, F]$ at 343.15 K.

Compound $[F, Br_2, F]$ stands out due to its density, attributed to the presence of six F and two Br atoms per molecule. Similarly, $[F, A, F]$ is also much denser than the other four alkenes due to its six F atoms. Density decreases in the order $[Bn, A, Bn] > [ME, A, ME] > [M, A, M] > [E, A, E]$, attributable to decreased intermolecular interactions caused by the different R group elements. These density values fall within the range of conventional solvents (0.654 – 1.4489 g cm⁻³, 298.15 K) and glycerol (1.473 g cm⁻³, 298.15 K) except for $[F, Br_2, F]$.

2.3 Viscosity

Understanding liquid viscosities is key in gas absorption processes. Elevated viscosity may reduce mass transfer rates and require extra contactor materials to manage rapid pressure drops along the contactor length. Viscosity values of (*E/Z*)-1,3-diether-2-alkenes, obtained from measurements and corrected COSMOtherm calculations over the range of $T = 293.15$ – 333.15 K, along with percentage errors, are shown in Table 4. While COSMOtherm reliably predicts density, its agreement with experimental viscosity calculations is less



Scheme 1 Synthesis route of symmetric (*E/Z*)-alkenes and additional reactions.



Table 2 Densities (ρ) of (*E/Z*)-1,3-diether-2-alkenes and [F, Br₂, F] with COSMOtherm calculations at different temperatures (*T*) and *P* = 101 kPa^a

<i>T</i> (K)	ρ_m^b (g cm ⁻³) (1) [M, A, M]	ρ_c^c (g cm ⁻³)	ρ_c^d (g cm ⁻³)	Error ^{e,f} (%)	ρ_m^b (g cm ⁻³) (2) [E, A, E]	ρ_c^c (g cm ⁻³)	ρ_c^d (g cm ⁻³)	Error ^{e,f} (%)
293.15	0.91092	0.91551	0.90572	(-0.50, 0.57)	0.87859	0.91013	0.89990	(-3.59, -2.43)
303.15	0.90062	0.90572	0.89634	(-0.57, 0.48)	0.86894	0.90080	0.89050	(-3.67, -2.48)
313.15	0.89024	0.89680	0.88690	(-0.74, 0.38)	0.85924	0.89171	0.88133	(-3.78, -2.57)
323.15	0.87972	0.88761	0.87781	(-0.90, 0.17)	0.84946	0.88262	0.87231	(-3.90, -2.69)
333.15	0.86906	0.87704	0.86703	(-0.92, 0.23)	0.83958	0.87203	0.86090	(-3.87, -2.54)
343.15	0.85828	0.86813	0.85821	(-1.15, 0.01)	0.82964	0.86331	0.85302	(-4.06, -2.82)
	(3) [ME, A, ME]				(4) [F, A, F]			
293.15	1.01276	1.02201	1.01303	(-0.91, 0.03)	1.33816	1.41601	1.38261	(-5.82, -3.32)
303.15	1.00354	1.01220	1.00321	(-0.86, 0.03)	1.32211	1.40251	1.36923	(-6.08, -3.56)
313.15	0.99431	1.00261	0.99350	(-0.83, 0.08)	1.30611	1.38922	1.35590	(-6.36, -3.81)
323.15	0.98504	0.99303	0.98390	(-0.81, 0.12)	1.28992	1.37591	1.34271	(-6.67, -5.12)
333.15	0.97574	0.98090	0.97081	(-0.53, 0.51)	1.27357	1.35961	1.32653	(-6.76, -4.16)
343.15	0.96640	0.97241	0.96332	(-0.62, 0.32)	1.25704	1.34750	1.31450	(-7.20, -4.57)
	(5) [Bn, A, Bn]				(6) [F, Br ₂ , F]			
293.15	1.03426	1.09342	1.08441	(-5.72, -4.85)	1.82520	1.95675	1.95892	(-7.21, -7.33)
303.15	1.02617	1.08371	1.07470	(-5.61, -4.73)	1.80682	1.93792	1.94006	(-7.26, -7.37)
313.15	1.01811	1.07403	1.06501	(-5.49, -4.61)	1.78848	1.91918	1.92129	(-7.31, -7.43)
323.15	1.01006	1.06431	1.05530	(-5.37, -4.48)	1.77007	1.90052	1.90260	(-7.37, -7.49)
333.15	1.00201	1.05202	1.04301	(-4.99, -4.09)	1.75164	1.88196	1.88402	(-7.44, -7.56)
343.15	0.99398	1.04330	1.03410	(-4.96, -4.04)	1.73314	1.86350	1.86552	(-7.52, -7.64)

^a Uncertainties are $u(T) = 0.01$ K and $u(\rho) = 0.00001$ (g cm⁻³). ^b Measured density. ^c COSMOtherm calculated density for the *E* and *R* structures. ^d COSMOtherm calculated density for the *Z* and *S* structures. ^e Error = $((\rho_m - \rho_c)/\rho_m) \times 100$ for each structure. ^f Error = $((\rho_m - \rho_c)/\rho_m) \times 100$ for each structure.

accurate. The classic Andrade equation ($\eta = a \cdot \exp(b/T)$) was used to fit the temperature-viscosity relationship,^{38,39} having performed well in similar cases. Table 5 presents the Andrade equation parameters: *a*, the pre-exponential factor, which is a liquid-specific constant, and *b/T*, the primary determinant of viscosity reduction as temperature increases. The strong correlation ($R^2 > 0.99$) confirms the model's robustness in accurately describing the behavior of symmetric (*E/Z*)-1,3-diether-2-alkenes.

Fig. 2 provides visual comparisons of the experimentally measured viscosity trends. Adding alkyl groups increases viscosity because longer alkyl chains enhance intermolecular dispersion forces. This increase in forces raises resistance to flow and can also cause entanglement, further restricting molecular mobility and increasing viscosity. The viscosities of [M, A, M] and [E, A, E] are approximately 50% lower than those of [ME, A, ME] and [F, A, F]. The latter two compounds contain additional ether groups and F atoms, which contribute to stronger intermolecular forces and greater molecular rigidity, resulting in higher viscosity. Interestingly, [Bn, A, Bn] displays the greatest viscosity, which is in contrast with the density changes observed in [E, A, E], [ME, A, ME], and [F, A, F]. This difference arises because the aromatic ring facilitates π - π interactions between adjacent molecules. These non-covalent interactions restrict molecular motion, leading to an increase in viscosity. The presence of the benzyl group significantly enhances viscosity compared to ether

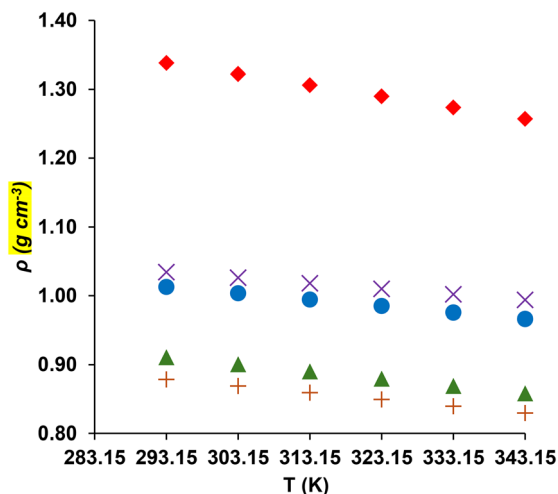


Fig. 1 Measured densities within the range of *T* = 293.15–343.15 K for (*E/Z*)-1,3-diether-2-alkenes; plus = [E, A, E]; triangle = [M, A, M]; circle = [ME, A, ME]; cross = [Bn, A, Bn]; diamond = [F, A, F].

Table 3 Parameters of the density-temperature linear fit ($\rho = -a \times T + b$) for compounds studied in this work within a temperature range of 293.15–354.15 K

Compound	<i>a</i> (10 ⁻⁴ g cm ⁻³ K)	<i>b</i> (g cm ⁻³)	<i>R</i> ²
[M, A, M]	10.528	1.220	0.9999
[E, A, E]	9.790	1.166	1.0000
[ME, A, ME]	9.272	1.285	1.0000
[F, A, F]	16.224	1.814	1.0000
[Bn, A, Bn]	8.056	1.270	1.0000
[F, Br ₂ , F]	18.412	2.365	1.0000



Table 4 Dynamic viscosities (η) of symmetric (*E/Z*)-1,3-diether-2-alkenes at temperatures (*T*) from 293.15 to 333.15 K and *p* = 101 kPa^a

<i>T</i> (K)	η_m^b (mPa s) (1) [M, A, M]	η_c^{cc} (mPa s)	η_c^{cd} (mPa s)	Error ^{e,f} (%)	η_m^b (mPa s) (2) [E, A, E]	η_c^{cc} (mPa s)	η_c^{cd} (mPa s)	Error ^{e,f} (%)
293.15	0.82	1.03	0.88	(−26.61, −7.32)	1.22	1.60	1.36	(−31.14, −11.48)
303.15	0.75	0.89	0.77	(−18.67, −2.67)	1.12	1.35	1.16	(−3.67, −2.48)
313.15	0.71	0.77	0.67	(−8.45, 5.63)	1.03	1.14	0.99	(−3.78, −2.57)
323.15	0.63	0.68	0.60	(−7.94, 4.76)	0.95	0.98	0.86	(−3.90, −2.69)
333.15	0.56	0.58	0.52	(−3.57, 7.14)	0.90	0.83	0.73	(−3.87, −2.54)
	(3) [ME, A, ME]				(4) [F, A, F]			
293.15	3.85	8.44	7.07	(−119.22, −83.64)	2.01	3.64	3.00	(−81.09, −49.25)
303.15	3.29	6.43	5.44	(−95.44, −65.35)	1.69	2.92	2.43	(−72.78, −43.79)
313.15	2.63	4.99	4.26	(−89.73, −14.82)	1.43	2.37	1.99	(−65.73, −39.16)
323.15	2.24	3.92	3.38	(−75.00, −50.90)	1.22	1.95	1.66	(−59.83, −36.02)
333.15	1.82	3.01	2.62	(−65.38, −43.96)	1.05	1.57	1.35	(−49.52, −28.71)
	(5) [Bn, A, Bn]							
293.15	8.25	73.18	62.37	(−787.03, −656.00)				
303.15	6.54	49.06	42.21	(−650.15, −545.03)				
313.15	5.27	33.69	29.25	(−539.27, −455.02)				
323.15	3.94	23.66	20.71	(−492.98, −419.04)				
333.15	3.27	16.04	14.17	(−390.51, −333.33)				

^a Temperature variance is ± 0.01 K. ^b Measured viscosity. ^c Corrected COSMOtherm viscosity for the *E* and *Z* structures, corrected viscosity (η_c) = $1.3 \times$ calculated viscosity by COSMOtherm (η_c). ^d Corrected COSMOtherm viscosity for the *E* and *Z* structures, corrected viscosity (η_c) = $1.3 \times$ calculated viscosity by COSMOtherm (η_c). ^e Error = $((\eta_m - \eta_c)/\eta_m) \times 100$ for the *E* and *Z* structures. ^f Error = $((\eta_m - \eta_c)/\eta_m) \times 100$ for the *E* and *Z* structures.

groups and F atoms. Comparing the viscosities of glycerol-derived 2° alcohols, ketones, and triethers, solvent viscosity follows the order $[R_1, 0, R_1] > [R_1, K, R_1] > [R_1, R_1, R_1] \gg [R_1, A, R_1]$,^{17,23} related to the presence or absence of H-bonding and intermolecular forces when 2° alcohols are converted to ketones or ethers, with further depression of molecular interactions due to alcohol elimination. It is important to note that the viscosity of [Bn, A, Bn] is not less than that of some of the $[R_1, 0, R_1]$, $[R_1, K, R_1]$, and $[R_1, R_1, R_1]$ solvents.

Viscosity is a crucial transport property of organic molecules, and is correlated with pressure drop and mass/heat transfer rates in gas absorption processes. Less viscous liquids are preferred, particularly in continuous absorption-stripping processes. To evaluate how the alkene group contributes to CO₂ absorption capacities in organic liquids, viscosity data for DMPEG from Li's group⁴⁰ are presented in Fig. 2. The viscosity ranking of the “green” physical solvents employed for CO₂ capture in our lab, as previously noted, is as follows: $[R_1, 0, R_1] > [R_1, K, R_1] > [R_1, R_1, R_1] \gg [R_1, A, R_1]$, excluding [Bn, A, Bn]. Fig. 2 illustrates that four

symmetric (*E/Z*)-1,3-diether-2-alkenes, apart from [Bn, A, Bn], demonstrate lower viscosities than DMPEG. This finding suggests that these liquids might lead to reduced energy costs for liquid transport and offer advantages for simplifying device design. Hence, the developed compounds would be competitive with DMPEG in CO₂ absorption, although we note that the presence of a C=C bond is not a common feature of organic liquids used in industrial CO₂ absorption processes.

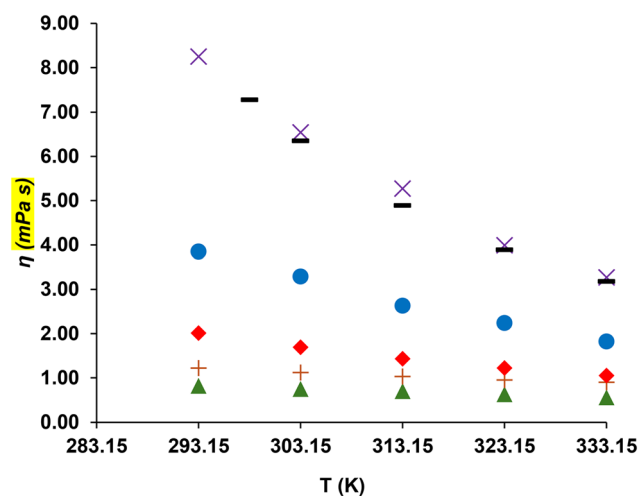


Fig. 2 Comparison of viscosity within the temperature range of 293.15–343.15 K for (*E/Z*)-1,3-diether-2-alkenes and DMPEG. Plus = [E, A, E]; triangle = [M, A, M]; circle = [ME, A, ME]; cross = [Bn, A, Bn]; diamond = [F, A, F]; dash = DMPEG.

Table 5 Viscosity–temperature equation ($\eta = a \exp(b/T)$) parameters for symmetric (*E/Z*)-1,3-diether-2-alkenes at 293.15–333.15 K

Compound	<i>a</i> (mPa s)	<i>b</i> (K)	<i>R</i> ²
[M, A, M]	3.4226×10^{-2}	0.931×10^3	0.9913
[E, A, E]	9.6825×10^{-2}	0.743×10^3	0.9963
[ME, A, ME]	0.7090×10^{-2}	1.848×10^3	0.9982
[F, A, F]	0.9004×10^{-2}	1.585×10^3	0.9948
[Bn, A, Bn]	0.3707×10^{-2}	2.259×10^3	0.9903



2.4 Refractive index (RI)

The RI of a molecule is a crucial indicator of its polarizability and is also used as a purity measure in organic chemistry.¹⁷ [R₁, A, R₁] alkenes exhibit similar RI values (1.4197–1.4435 at 298.15 K), except for [F, A, F] (1.3476) and [F, Br₂, F] (1.4134). The RI of [Bn, A, Bn] (1.54426) is close to the RI of benzyl alcohol (1.539). These values fall within the range of conventional solvents (1.32–1.54) and glycerol (1.473) and decrease slightly with increasing temperature. From [M, A, M] to [E, A, E] and [ME, A, ME], longer alkyl chains result in higher refractivity as their larger electron clouds are more easily polarized, and their stronger intermolecular interactions contribute to a denser optical medium. F atoms exhibit the highest electronegativity and the smallest atomic radius among the halogens. This characteristic leads to strong inductive effects that diminish the overall polarizability of molecules containing fluorine atoms, *i.e.*, [F, A, F]. In contrast, Br atoms are considerably larger and possess higher polarizability ([F, Br₂, F]). The increased polarizability of the C–Br bond results in a higher refractive index, while the greater atomic mass of Br further enhances its ability to bend light (Table 6).

2.5 CO₂ solubility

CO₂ absorption data were collected for [F, A, F] at four different temperatures ($T = 303.15, 318.15, 333.15,$ and 348.15 K) under low pressures ($P = 2$ – 10 atm). Table 7 displays the CO₂ partial pressures and the corresponding CO₂ molar ratios, calculated using the data collected at each absorption equilibrium. To investigate the relationship between X_{CO_2} and CO₂ partial pressure (P), the information from Table 7 is graphed in Fig. 3. Table 8 shows the absorption data, including Henry's constant, volumetric concentration (S_v), and molality (S_m). The slope (m) represents X_{CO_2} relative to CO₂ partial pressure, with the average absolute percent deviation (AAPD)²⁴ values being small (0.13–0.69%) and correlation coefficients (R^2) between 0.99 and 1.00, indicating a strong linear relationship between X_{CO_2} in solvent and CO₂ partial pressure. It is worth noting that smaller Henry's constant (*i.e.*, $P = H_{\text{CO}_2} \cdot X_{\text{CO}_2}$) values indicate higher CO₂ solubility in a given solvent. Previous studies indicate that H_{CO_2} values decrease in the order: alcohol > ketone > triether at the same temperature.^{20,22,23} This trend occurs because the removal

of H-bonds weakens solvent–solvent interactions while strengthening solvent–gas (solute) interactions, thereby increasing CO₂ solubility in ketones compared to their corresponding alcohols. Additionally, the highest H_{CO_2} values are attributed to the presence of extra ether O atoms.^{20,22,23} The CO₂ absorption performance of diglyme, a commonly used DMPEG oligomer ($H_{\text{CO}_2} = 4.21$ MPa, at 303.15 K)³⁵ was compared with that of 1-*n*-hexyl-3-methylimidazolium bis(trifluoromethyl sulfonyl) imide ([C₆mim][Tf₂N]), a well-characterized IL ($H_{\text{CO}_2} = 3.90$ MPa, at 303.15 K).⁴¹ Additionally, previously studied glycerol-derived liquids, including [F, O, F] ($H_{\text{CO}_2} = 4.50$ MPa at 303.15 K),²⁰ [F, K, F] ($H_{\text{CO}_2} = 4.47$ MPa at 303.15 K),²² and [F, ME, F] ($H_{\text{CO}_2} = 3.0.6$ MPa, at 303.15 K),²² were also assessed. Among these, [F, A, F] ($H_{\text{CO}_2} = 3.47$ MPa, at 303.15 K) demonstrated good CO₂ solubility, likely due to its further reduced H-bonding.

2.6 Miscibility evaluation

The synthesized (*E/Z*)-1,3-diether-2-alkenes exhibit low viscosity and [F A F] was shown to have a high CO₂ absorption capacity. The miscibility of these liquids with common organic solvents and water is also of interest. A miscibility chart was developed for (*E/Z*)-1,3-diether-2-alkenes with commonly used solvents. As seen in Table S4.1,[†] all these alkenes are insoluble in water due to their nonpolar nature, while water is highly polar. Conversely, all these alkenes are soluble in organic solvents, ranging from hexanes (nonpolar) to toluene, dichloromethane (CH₂Cl₂), diethyl ether (Et₂O), tetrahydrofuran (THF), acetone, dimethylformamide (DMF), and dimethyl sulfoxide (DMSO) (most polar). The high solubility of these alkenes in conventional solvents may be attributed to their slight polarity differences.

2.7 Dipole moment calculations

Table S3.5[†] presents the calculated dipole moments for symmetric (*E/Z*)-1,3-diether-2-alkenes, which range from 1.62 to 4.86 D at room temperature, with minor differences observed between the *E* and *Z* isomers. Specifically, the dipole moment for the (*E/Z*)-[F, A, F] structure was calculated to be 4.86 D for the *E* isomer and 4.70 D for the *Z* isomer. The presence of fluorine atoms significantly increases permittivity, resulting in the highest dipole moment observed

Table 6 Refractive index (n_D) of symmetric (*E/Z*)-1,3-diether-2-alkenes at $T = 293.15$ and 298.15 K and $P = 1$ atm^a

Compound	Temperature (K)	Refractive index (n_D)	Temperature (K)	Refractive index (n_D)
[M, A, M]	293.15 K	1.42050	298.15 K	1.41970
[E, A, E]	293.15 K	1.42320	298.15 K	1.42100
[F, A, F]	293.15 K	1.35040	298.15 K	1.34760
[F, Br ₂ , F]	293.15 K	1.41700	298.15 K	1.41340
[ME, A, ME]	293.15 K	1.44470	298.15 K	1.44350
[Bn, A, Bn]	293.15 K	1.54460	298.15 K	1.54426

^a Uncertainty for temperature is $u(T) = 0.01$ K.



Table 7 CO₂ absorption data for [F, A, F]^a

$T = 303.15\text{ K}$		$T = 318.15\text{ K}$		$T = 333.15\text{ K}$		$T = 348.15\text{ K}$	
P/MPa	$X_{\text{CO}_2}/(\text{mol mol}^{-1})$	P/MPa	$X_{\text{CO}_2}/(\text{mol mol}^{-1})$	P/MPa	$X_{\text{CO}_2}/(\text{mol mol}^{-1})$	P/MPa	$X_{\text{CO}_2}/(\text{mol mol}^{-1})$
0.211	0.0640	0.230	0.0601	0.241	0.0571	0.255	0.0545
0.426	0.1203	0.461	0.1136	0.492	0.1080	0.531	0.1062
0.626	0.1728	0.672	0.1623	0.714	0.1543	0.731	0.1471

^a Standard uncertainties are $u(T) = 0.5\text{ K}$, $u(P) = 0.005\text{ MPa}$, and $u(x) = 0.002$.

for [F, A, F] among the alkenes studied. As the alkyl chain length increases, the polarity of these alkenes decreases, consistent with the trend observed for [M, A, M] (3.16 D, 2.30 D), [E, A, E] (3.11 D, 2.40 D), and [ME, A, ME] (1.79 D, 1.62 D). High dipole moments typically indicate strong interactions with polar solvents, leading to increased solubility. For instance, [F, A, F], which exhibits the highest dipole moment (4.86 and 4.70 D for the *E* and *Z* isomers, respectively), is expected to be highly soluble in a polar organic solvent. Dipole moments may also influence how molecules interact with electrophiles and nucleophiles. A highly polar compound such as [F, A, F] may present strong electrophilic or nucleophilic characteristics, depending on the distribution of electron density. In contrast, the least polar molecule, [ME, A, ME], may have reduced reactivity under polar reaction conditions due to weaker charge separation. It is important to note that the calculated dipole moment is influenced by the local environment, whether in the gas or liquid phase, and whether thermal motion is considered. The calculated dipole moment values fall within the typical range of conventional solvents (0.10–4.10 D),²⁴ spanning from nonpolar hexanes to highly polar DMSO. These calculated dipole moments enable better understanding as to why (*E/Z*)-1,3-diether-2-alkenes were miscible with all of the selected conventional solvents. The glycerol-derived liquids with the highest CO₂ absorption

capacity – [R₁, 0, R₁], [R₁, K, R₁], [R₁, R₁, R₁], and [R₁, A, R₁] – were selected for a comparative analysis of their dipole moments. The calculated dipole moments for these solvents were as follows: [F, 0, F] (4.09 D),²⁰ [F, K, F] (4.34 D),²² [F, ME, F] (5.86 D),²² and [F, A, F] (*E* – 4.86 D, *Z* – 4.70 D). A positive correlation was observed between dipole moments and CO₂ absorption capacity, suggesting that organic liquids with higher dipole moments tend to exhibit greater CO₂ absorption.

3 Conclusions

A straightforward three-step method for synthesizing novel symmetric (*E/Z*)-alkenes ([M, A, M], [E, A, E], [ME, A, ME], [F, A, F], and [Bn, A, Bn]) based on a glycerol skeleton has been developed and characterized for the first time. Density and viscosity data were obtained over the temperature range of 293.15 to 343.15 & 333.15 K. Density data were fitted to a linear equation for reliable predictions ($R^2 = 0.9999$). In contrast, viscosity data were fitted to an exponential equation ($R^2 > 0.99$). All five compounds showed relatively low viscosity compared to [R₁, 0, R₁], [R₁, K, R₁], [R₁, R₁, R₁], and DMPEG. It is worth mentioning that the viscosity of [Bn, A, Bn] is not less than that of some of the [R₁, 0, R₁], [R₁, K, R₁], and [R₁, R₁, R₁] liquids. COSMOtherm calculations applied for comparison showed good reliability for density simulations, though viscosity predictions could be improved. Henry's constants were measured under modest pressure and then extrapolated over the range of $T = 273.15$ to 353.15 K with minor errors. [F, A, F] exhibited good CO₂ capacity and low viscosity. The five alkenes showed consistency and good compatibility with common organic solvents, and the calculated dipole moments appear to explain this behavior. Furthermore, these alkenes can be utilized as platform molecules for halogenation, as demonstrated in the conversion of [F, A, F] to [F, Br₂, F], providing new and unique intermediates for synthesizing molecules using glycerol-derived carbon atoms. Other potential avenues for utilizing these alkenes to make new molecules include alkylation at the vinyl position or oxidative cleavage. The synthesized (*E/Z*)-1,3-diether-2-alkene molecules, derived from “activated molecular” forms, could have a role in promoting environmental sustainability in green chemistry, and they offer new applications for utilizing excess glycerol. Future expansion of these studies include studying the separation of *E* and *Z* isomers, recharacterizing the individual isomers' properties, comparing them with calculation results,

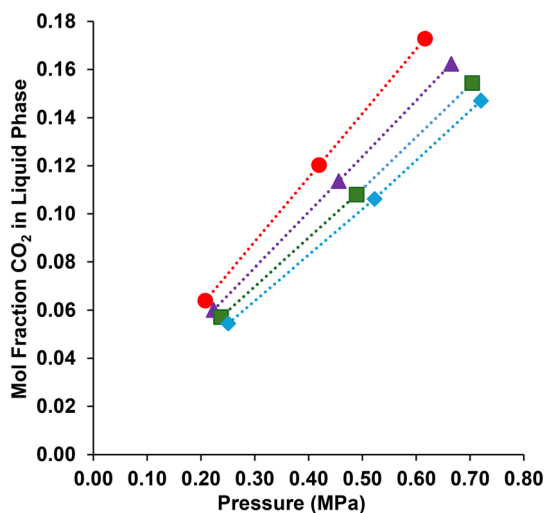


Fig. 3 CO₂ absorption data for [F, A, F]. $T = 303.15\text{ K}$ (circle); $T = 318.15\text{ K}$ (triangle); $T = 333.15\text{ K}$ (square); $T = 348.15\text{ K}$ (diamond).



Table 8 CO₂ solubility parameters of [F, A, F] studied at relevant temperatures^{a,b}

Compound	<i>T</i> (K)	<i>m</i> (10 ⁻² atm ⁻¹)	AAPD%	<i>R</i> ²	<i>H</i> _{CO₂} (atm)	<i>S</i> _v (cm ³ (STP) cm ⁻³ atm ⁻¹)	<i>S</i> _m (mol kg ⁻¹ atm ⁻¹)
[F, A, F]	303.15	2.878	0.134	1.0000	34.75 ± 0.8	3.04 ± 0.05	0.127 ± 0.002
	318.15	2.569	0.216	1.0000	38.92 ± 0.7	2.57 ± 0.04	0.114 ± 0.002
	333.15	2.288	0.322	0.9996	43.70 ± 1.5	2.31 ± 0.02	0.102 ± 0.002
	348.15	2.031	0.688	0.9995	49.20 ± 0.2	1.90 ± 0.05	0.092 ± 0.001

^a Uncertainties are $u(T) = 0.01$ K, $u(m) = 0.001$, $u(\text{AAPD}) = 0.001$ and $u(R^2) = 0.0001$. ^b *m* is the inverse of Henry's constant (*i.e.*, $m = 1/H_{\text{CO}_2}$).

and synthesizing novel asymmetric (*E/E/Z/Z*) alkenes by starting from glycidyl ethers and using the same reaction conditions. This work will open opportunities to create new classes of chemical intermediates.

4 Experimental

4.1 Materials

Dichloromethane (CH₂Cl₂, 99.5% min), methanol (MeOH, 99.8% min), ethanol (EtOH, 99% min), acetone (99.5% min), sodium hydroxide (NaOH, 97%), *N,N*-dimethylformamide (DMF, 99.8% min), and sodium bicarbonate (NaHCO₃, 99.7% min) were purchased from VWR. (±)-ECH (99%), 2,2,2-trifluoroethanol (CF₃CH₂OH, 99%), 2-methoxyethanol (CH₃-OCH₂CH₂OH, 99%), benzyl alcohol (BnOH, 98%), and chloroform-*d* (CDCl₃-*d*, 99.8%) were purchased from BeanTown Chemical; MsCl (98%) was purchased from Thermo Scientific Chemicals; toluene (99.8%) from Alfa Aesar; ACS grade tetrahydrofuran (THF, 99.8% min) and hexanes (mixture of isomers, 99.5% min) were purchased from Avantor; ACS grade dimethyl sulfoxide (DMSO, 99.8% min) and anhydrous magnesium sulfate (MgSO₄, 98.0% min) were purchased from EMD Millipore Corporation; anhydrous diethyl ether (Et₂O, 99.0% min) was purchased from J.T. Baker; triethylamine (Et₃N, 99.5% min) was purchased from Oakwood Chemical; DMSO-*d*₆ (99% with 0.05% V/V TMS) was purchased from Cambridge Isotope Laboratories; molecular sieves (3 Å, 3.2 mm pellets) were purchased from Sigma-Aldrich; and CO₂ (99.999%) was purchased from Airgas. All chemicals were used without further purification.

4.2 Synthesis

The synthetic routes for the compounds studied in this work are illustrated in Scheme 1, with all reactions performed at molar scales. This study follows a three-step synthesis starting from ECH. The overall isolated yields for [M, A, M], [E, A, E], [ME, A, ME], [F, A, F], and [Bn, A, Bn] were 30.3%, 35.9%, 56.8%, 53.8%, and 61.7%, respectively. Each step was purified through meticulous distillation and dried with 3 Å molecular sieves. Detailed synthetic procedures and compound characterization data are provided in the ESI.†

4.3 Density measurements

Density measurements for the five symmetric (*E/Z*)-1,3-diether-2-alkenes and [F Br₂ F] were conducted using a

Mettler Toledo DM45 Delta Range densitometer at 1 atm within the temperature range of 293.15–343.15 K with a temperature error of ±0.05 K, controlled automatically with 10.00 K increments, similar to previous work.⁴² Calibrations were performed using the manufacturer's water standards. The sample cell was cleaned before and after the sample injection with air purging, acetone rinsing, and air drying. All samples were stored over 3 Å molecular sieves for 48 h prior to density measurements.

4.4 Dynamic viscosity measurements

Dynamic viscosities of the five symmetric (*E/Z*)-1,3-diether-2-alkenes were measured using a Brookfield DV-II+ Pro viscometer with an “ULA” spindle and jacketed sample cell at 1 atm within the temperature range of 293.15–333.15 K with a temperature error of ±0.01 K, controlled with a Brookfield TC-602P circulating bath with 10.00 K increments, similar to previous work.⁴³ The sample cell was cleaned with acetone rinsing and air blowing before and after each measurement. The samples were stored over 3 Å molecular sieves for 48 h before each measurement.

4.5 Refractive index measurements

RI measurements for the five symmetric (*E/Z*)-1,3-diether-2-alkenes and [F, Br₂, F] were conducted using a Mettler Toledo DM45 Delta Range refractive index meter at 1 atm and 293.15 K and 298.15 K, controlled automatically at each temperature. Calibrations were performed using the manufacturer's water standards. The sample cell was cleaned with acetone rinsing and air blowing before and after each measurement. The samples were stored over 3 Å molecular sieves for 48 h before each measurement. Measurement of each compound was performed in triplicate.

4.6 CO₂ absorption measurements

CO₂ solubility in [F, A, F] was measured following a previously published method.³⁵ A 100 mL glass pressure vessel (#8648-136, Ace Glass) with a #25 threaded fitting and a front-sealing PTFE cap, featuring a 1/4 in NPT tap, served as the reaction cell. The system was operated at pressures between 2 and 10 atm. The pressure was monitored using a Baratron absolute capacitance manometer (722B, MKS Instruments) with a 1–10 000 Torr range and displayed digitally using a PDR2000 (MKS Instruments) to maintain equilibrium under varying test conditions. CO₂ partial



pressure and the closed system's weight were recorded upon reaching vapor-liquid equilibrium (VLE), indicated by the stable pressure gauge reading each time CO₂ was added, with temperature increasing from 303.15 to 348.15 K in 15 K increments.

4.7 Miscibility test

Miscibility tests involved conventional solvents (Table S4.1†) and developed five symmetric (*E/Z*)-1,3-diether-2-alkenes. Miscibility was determined visually. 5 mL of each liquid was injected into a 20 mL vial, mixed *via* vibration for 5 min, and left static for 30 min. A solvent pair was deemed “miscible” if the mixture was clear without heterogeneous phases; otherwise, it was “immiscible” if the mixture was not clear or had nonuniform parts observed.

4.8 Computational methods

Calculations were performed to systematically analyze the thermophysical properties of the experimentally studied symmetric (*E/Z*)-1,3-diether-2-alkenes. Using Gaussian 16,³⁷ we optimized the geometries of the solvent compounds in vacuum with the BP86 functional^{44,45} and the TZVP basis set.⁴⁶ To generate COSMO files, we performed single-point energy calculations with the above-mentioned basis set and functional, applying the COSMO-RS solvation model.^{47,48} We then conducted all COSMO calculations in COSMOtherm (BIOVIA COSMOtherm, Release 2020)³⁶ at the TZVP level to compute the densities (ρ), vapor pressures (P^*), viscosities (η), dipole moments (μ), and enthalpies of vaporization (ΔH) of each solvent compound over a temperature range of 10–70 °C. COSMOtherm employs COSMO-RS – widely considered as the most accurate quantum-chemistry-based solvation model,^{49,50} and offering a favorable balance between accuracy and computational efficiency. Previous studies have demonstrated that COSMOtherm is a practical and accurate tool for predicting thermophysical properties of solvent compounds, making it a reliable choice for comparative analysis.^{23–25,50} COSMOtherm however neglects the effect of explicit solvent molecules, limiting its accuracy especially in the presence of strong or directional solvent–solute interactions. While explicit solvation methods provide greater accuracy, their high computational cost makes them impractical for this study. Detailed calculation data can be found in the ESI†

Data availability

The data supporting this article have been included as part of the ESI†

Conflicts of interest

There are no conflicts to declare.

Acknowledgements

Support from the U.S. National Science Foundation (EFMA-2029387) is gratefully acknowledged. G. O. would like to acknowledge the financial support from the University of Alabama Graduate School as a Graduate Council Fellow. The images within the TOC graphic were created by the authors using AI generative software (Adobe Firefly). The authors' university has a license for Adobe Firefly and terms of use associated with the software are being followed. All other images/photographs were fully created by the authors.

References

- 1 C. A. G. Quispe, C. J. R. Coronado and J. A. Carvalho, Glycerol: Production, consumption, prices, characterization and new trends in combustion, *Renewable Sustainable Energy Rev.*, 2013, **27**, 475–493.
- 2 H. W. Tan, A. R. A. Aziz and M. K. Aroua, Glycerol production and its applications as a raw material: A review, *Renewable Sustainable Energy Rev.*, 2013, **27**, 118–127.
- 3 G. Lingua, G. Depraetere, J. Wang, J. E. Bara, M. Forsyth and D. Mecerreyes, Solvate ionic liquids based on branched glymes enabling high performance lithium metal batteries, *J. Power Sources*, 2024, **624**, 235535.
- 4 A. E. Díaz-Alvarez, J. Francos, B. L. Barreira, P. Crochet and V. Cadierno, Glycerol and derived solvents: New sustainable reaction media for organic synthesis, *Chem. Commun.*, 2011, **47**, 6208–6227.
- 5 D. L. Sun, Y. Yamada, S. Sato and W. Ueda, Glycerol as a potential renewable raw material for acrylic acid production, *Green Chem.*, 2017, **19**, 3186–3213.
- 6 M. Ayoub and A. Z. Abdullah, Critical review on the current scenario and significance of crude glycerol resulting from biodiesel industry towards more sustainable renewable energy industry, *Renewable Sustainable Energy Rev.*, 2012, **16**, 2671–2686.
- 7 D. T. Johnson and K. A. Taconi, The glycerin glut: Options for the value-added conversion of crude glycerol resulting from biodiesel production, *Environ. Prog.*, 2007, **26**, 338–348.
- 8 A. Almena and M. Martín, Technoeconomic analysis of the production of epichlorohydrin from glycerol, *Ind. Eng. Chem. Res.*, 2016, **55**, 3226–3238.
- 9 M. Sutter, D. E. Silva, N. Duguet, Y. Raoul, E. Métay and M. Lemaire, Glycerol ether synthesis: A bench test for green chemistry concepts and technologies, *Chem. Rev.*, 2015, **115**, 8609–8651.
- 10 P. Anastas and N. Eghbali, Green chemistry: Principles and practice, *Chem. Soc. Rev.*, 2010, **39**, 301–312.
- 11 V. Hessel, N. N. Tran, M. R. Asrami, Q. D. Tran, N. V. Long, M. E. Gelonch, J. O. Tejada, S. Linke and K. Sundmacher, Sustainability of green solvents - Review and perspective, *Green Chem.*, 2022, **24**, 410–437.
- 12 E. Santacesaria, R. Tesser, M. D. Serio, L. Casale and D. Verde, New process for producing epichlorohydrin via



- glycerol chlorination, *Ind. Eng. Chem. Res.*, 2010, **49**, 964–970.
- 13 I. V. Andreeva, V. V. Turovtsev, S. Qian, J. E. Bara and S. P. Verevkin, Biofuel additives: Thermodynamic studies of glycerol ethers, *Ind. Eng. Chem. Res.*, 2022, **61**, 15407–15413.
 - 14 J. F. Izquierdo, M. Montiel, I. Palés, M. Villarrubia, M. Izquierdo, M. P. Hermo and X. Ariza, Fuel additives from glycerol etherification with light olefins: State of the art, *Renewable Sustainable Energy Rev.*, 2012, **16**, 6717–6724.
 - 15 J. I. García, H. G. Marín, J. A. Mayoral and P. Pérez, Green solvents from glycerol. Synthesis and physico-chemical properties of alkyl glycerol ethers, *Green Chem.*, 2010, **12**, 426–434.
 - 16 R. Lebeuf, E. Illous, C. Dussenne, V. Molinier, E. D. Silva, M. Lemaire and J. M. Aubry, Solvo-surfactant properties of dialkyl glycerol ethers: Application as eco-friendly extractants of plant material through a novel hydrotropic cloud point extraction (HCPE) process, *ACS Sustainable Chem. Eng.*, 2016, **4**, 4815–4823.
 - 17 A. L. Duaso, P. Pérez, J. A. Mayoral, J. I. Garcia and E. Pires, Glycerol-derived solvents: Synthesis and properties of symmetric glyceryl diethers, *ACS Sustainable Chem. Eng.*, 2019, **7**, 13004–13014.
 - 18 A. L. Duaso, S. G. Barberán, J. A. Mayoral, J. I. Garcia and E. Pires, Readily scalable methodology for the synthesis of nonsymmetric glyceryl diethers by a tandem acid-/base-catalyzed process, *Org. Process Res. Dev.*, 2020, **24**, 154–162.
 - 19 S. N. T. Khadzhibekov, S. R. A. Sultankulov and C. S. Kadyrov, Some aspects of synthesis of 1,3-dialkoxy-2-propanols, *Dokl. Akad. Nauk UzSSR*, 1985, **3**, 40–41.
 - 20 S. Qian, X. Y. Liu, G. P. Dennis, C. H. Turner and J. E. Bara, Properties of symmetric 1,3-diethers based on glycerol skeletons for CO₂ absorption, *Fluid Phase Equilib.*, 2020, **521**, 112718.
 - 21 Z. S. Pour, P. S. Shinde, J. Wang, C. Woods, S. Taylor, S. Chatterjee and J. E. Bara, 1,3-Diether-2-methacrylates with glycerol skeletons: Tunable resins for stereolithography 3D printing, *Polym. Chem.*, 2025, DOI: [10.1039/D5PY00198F](https://doi.org/10.1039/D5PY00198F), Accepted Manuscript.
 - 22 S. Qian, X. Y. Liu, C. H. Turner and J. E. Bara, Synthesis and properties of symmetric glycerol-derived 1,2,3-triethers and 1,3-diether-2-ketones for CO₂ absorption, *Chem. Eng. Sci.*, 2022, **248**, 117150.
 - 23 S. Qian, X. Y. Liu, C. H. Turner and J. E. Bara, Glycerol-derived solvents containing two or three distinct functional groups enabled by trifluoroethyl glycidyl ether, *AIChE J.*, 2022, **68**, e17533.
 - 24 S. Qian, X. Y. Liu, V. N. Emel'yanenko, P. Sikorski, I. Kammakakam, B. S. Flowers, T. A. Jones, C. H. Turner, S. P. Verevkin and J. E. Bara, Synthesis and properties of 1,2,3-trimethoxypropane: A glycerol-derived green solvent candidate, *Ind. Eng. Chem. Res.*, 2020, **59**, 20190–20200.
 - 25 S. Chatterjee, S. Qian, A. Soyemi, T. Szilvasi and J. E. Bara, Synthesis and properties of 2-halo-1,3-diether-propanes: Diversifying the range of functionality in glycerol-derived compounds, *Ind. Eng. Chem. Res.*, 2023, **62**, 2959–2967.
 - 26 Z. Y. Zakaria, N. A. S. Amin and J. Linnekoski, A perspective on catalytic conversion of glycerol to olefins, *Biomass Bioenergy*, 2013, **55**, 370–385.
 - 27 J. P. Gujar and B. Modhera, A review on catalytic conversion of biodiesel derivative glycerol to bio olefins, *Mater. Today: Proc.*, 2022, **72**, 2723–2730.
 - 28 G. H. Huang, R. Guillot, C. Kouklovsky, B. Maryasin and A. Torre, Diastereo and enantioselective inverse-electron-demand diels-alder cycloaddition between 2-pyrones and acyclic enol ethers, *Angew. Chem., Int. Ed.*, 2022, **61**, e202208185.
 - 29 R. H. Hall and E. S. Stern, Alpha-beta-unsaturated aldehydes and related compounds .7. Thermal fission of 1-1-3-trialkoxypropanes, *J. Chem. Soc.*, 1955, 2657–2666.
 - 30 S. J. Gould and B. O. Remillard, Vinyl deprotonation in preference to allyl deprotonation. The reaction of 1,3-dibutoxypropene with t-butyllithium, *Tetrahedron Lett.*, 1978, **19**, 4353–4356.
 - 31 S. S. Navarro, M. Mon, A. D. Carbó, R. Greco, J. S. Quesada, E. E. Ferri and A. L. Pérez, Parts-per-million of ruthenium catalyze the selective chain-walking reaction of terminal alkenes, *Nat. Commun.*, 2022, **13**, 2831.
 - 32 M. Amaral, E. A. Crespo, C. Dariva, L. F. Vega, P. J. Carvalho and J. A. P. Coutinho, High-pressure solubility of CO₂ in glymes, *Fuel*, 2018, **219**, 120–125.
 - 33 H. Sugiyama and Y. Hattori, Selective and enhanced CO₂ adsorption on fluorinated activated carbon fibers, *Chem. Phys. Lett.*, 2020, **758**, 137909.
 - 34 S. Qian, J. D. Leah, S. Chatterjee, A. Soyemi, T. Szilvasi and J. E. Bara, Properties of imidazolium ionic liquids with glycerol-derived functional groups, *J. Chem. Eng. Data*, 2022, **67**, 1905–1914.
 - 35 B. S. Flowers, M. S. Mittenenthal, A. H. Jenkins, D. A. Wallace, J. W. Whitley, G. P. Dennis, M. Wang, C. H. Turner, V. N. Emel'yanenko, S. P. Verevkin and J. E. Bara, 1,2,3-Trimethoxypropane: A glycerol-derived physical solvent for CO₂ absorption, *ACS Sustainable Chem. Eng.*, 2017, **5**, 911–921.
 - 36 BIOVIA COSMOtherm, Dassault Systèmes. Available online: <https://www.3ds.com/products/biovia/cosmo-rs/cosmotherm> (accessed on 28 April 2025).
 - 37 M. J. Frisch, G. W. Trucks, H. B. Schlegel, G. E. Scuseria, M. A. Robb, J. R. Cheeseman, G. Scalmani, V. Barone, G. A. Petersson and H. Nakatsuji, *Gaussian 16 Rev. C.01*, Gaussian, Inc., Wallingford, CT, USA, 2016.
 - 38 E. N. D. C. Andrade, A theory of the viscosity of liquids, -Part I, *Philos. Mag.*, 1934, **17**, 497–511.
 - 39 E. N. D. C. Andrade, A theory of the viscosity of liquids, -Part II, *Philos. Mag.*, 1934, **17**, 693–732.
 - 40 J. L. Li, M. Mundhwa and A. Henni, Volumetric properties, viscosities, refractive indices, and surface tensions for aqueous genosorb 1753 solutions, *J. Chem. Eng. Data*, 2007, **52**, 955–958.
 - 41 A. Finotello, J. E. Bara, D. Camper and R. D. Noble, Room-temperature ionic liquids: Temperature dependence of gas



- solubility selectivity, *Ind. Eng. Chem. Res.*, 2008, **47**, 3453–3459.
- 42 M. S. Shannon and J. E. Bara, Properties of alkylimidazoles as solvents for CO₂ capture and comparisons to imidazolium-based ionic liquids, *Ind. Eng. Chem. Res.*, 2011, **50**, 8665–8677.
 - 43 J. E. Bara, A. Finotello, J. W. Magee, S. Qian, K. E. O'Harra, G. P. Dennis and R. D. Noble, 110th Anniversary: Properties of imidazolium-based ionic liquids bearing both benzylic and alkyl substituents, *Ind. Eng. Chem. Res.*, 2019, **58**, 17956–17964.
 - 44 A. D. Becke, Density-functional exchange-energy approximation with correct asymptotic-behavior, *Phys. Rev. A: At., Mol., Opt. Phys.*, 1988, **38**, 3098–3100.
 - 45 J. P. Perdew, Density-functional approximation for the correlation energy of the inhomogeneous electron gas, *Phys. Rev. B: Condens. Matter Mater. Phys.*, 1986, **33**, 8822.
 - 46 A. Schäfer, C. Huber and R. Ahlrichs, Fully optimized contracted Gaussian basis sets of triple zeta valence quality for atoms Li to Kr, *J. Chem. Phys.*, 1994, **100**, 5829–5835.
 - 47 F. Eckert and A. Klamt, Fast solvent screening via quantum chemistry: COSMO-RS approach, *AIChE J.*, 2002, **48**, 369–385.
 - 48 A. Klamt and F. Eckert, COSMO-RS: A novel and efficient method for the a priori prediction of thermophysical data of liquids, *Fluid Phase Equilib.*, 2000, **172**, 43–72.
 - 49 A. Klamt, The COSMO and COSMO-RS solvation models, *Wiley Interdiscip. Rev.:Comput. Mol. Sci.*, 2011, **1**, 699–709.
 - 50 J. Glüge and M. Scheringer, Evaluation of physicochemical property data in the ECHA database, *J. Phys. Chem. Ref. Data*, 2023, **52**, 043101.

